

Accepted Manuscript

Thixotropic gel electrolyte containing poly(ethylene glycol) with high zinc ion concentration for the secondary aqueous Zn/LiMn₂O₄ battery

Aly Mitha, Hongyu Mi, Wenhan Dong, In Sik Cho, Jessica Ly, Skylar Yoo, Sydney Bang, Tuan K.A. Hoang, P. Chen



PII: S1572-6657(19)30023-2
DOI: <https://doi.org/10.1016/j.jelechem.2019.01.014>
Reference: JEAC 12844
To appear in: *Journal of Electroanalytical Chemistry*
Received date: 10 October 2018
Revised date: 3 January 2019
Accepted date: 7 January 2019

Please cite this article as: Aly Mitha, Hongyu Mi, Wenhan Dong, In Sik Cho, Jessica Ly, Skylar Yoo, Sydney Bang, Tuan K.A. Hoang, P. Chen, Thixotropic gel electrolyte containing poly(ethylene glycol) with high zinc ion concentration for the secondary aqueous Zn/LiMn₂O₄ battery. *J. Electroanal. Chem.* (2019), <https://doi.org/10.1016/j.jelechem.2019.01.014>

This is a PDF file of an unedited manuscript that has been accepted for publication. As a service to our customers we are providing this early version of the manuscript. The manuscript will undergo copyediting, typesetting, and review of the resulting proof before it is published in its final form. Please note that during the production process errors may be discovered which could affect the content, and all legal disclaimers that apply to the journal pertain.

**Thixotropic Gel Electrolyte containing Poly(ethylene glycol) with
High Zinc Ion Concentration for the Secondary Aqueous
Zn/LiMn₂O₄ Battery**

Aly Mitha,^a Hongyu Mi,^b Wenhan Dong,^a In Sik Cho,^a Jessica Ly,^a Skylar Yoo,^a
Sydney Bang,^a Tuan K. A. Hoang,^a P. Chen^{a*}

^aDepartment of Chemical Engineering, University of Waterloo, 200 University
Avenue West, Waterloo, Ontario N2L 3G1, Canada.

^bXinjiang Uygur Autonomous Region Key Laboratory of Coal Clean Conversion and
Chemical Engineering Process, Xinjiang University, Urumqi, PR China

*Corresponding author.

Email: p4chen@uwaterloo.ca

Tel.: +1-519-888-4567 ext. 35586

Abstract

We have designed an aqueous gel electrolyte containing fumed silica as the thixotropic gelling agent and poly(ethylene glycol) (MW = 300 g·mol⁻¹) as the non-thixotropic gelling agent. Poly(ethylene glycol) is also the dendrite suppressor and the corrosion inhibitor. Both PEG300 and fumed silica can inhibit dendrite formation, shown by chronoamperometry results and ex-situ scanning electron microscopy images. Furthermore, the corrosion current density on the Zn anode in the 4wt.%FS-1wt.%PEG300 gel electrolyte is 27% less than that of the Zn in the reference aqueous

electrolyte. Secondary Zn/LiMn₂O₄ batteries using the 4wt.%FS-1wt.%PEG300 gel electrolyte exhibit higher cyclability (12% and 39% higher capacity retention, after 300 and 1000 cycles, in Swagelok and large cells, respectively) than those using the reference aqueous electrolyte. The vast improvements in cycling performance, reliability, and higher resistance to premature failure makes the PEG-FS gel a much better alternative to liquid electrolytes for maintenance-free energy storage applications.

Keywords: Zinc Anode, Aqueous Electrolyte, Gel Electrolyte, Dendrite, Corrosion.

1. Introduction

Zinc (specific reversible capacity: $820 \text{ A}\cdot\text{h}\cdot\text{kg}^{-1}$) is a low cost first order electrode and an environmentally-friendly material [1]. It has been used as an anode in very wide range of rechargeable aqueous batteries such as Zn-Ni, Zn-Metal Oxide, Zn-polymer, Zn-Air, and Zn-ion systems [2–19]. Despite its many advantages, secondary zinc batteries have not yet been commercialized to the same extent as Li-ion technologies due to some problems which are fundamentally related to zinc itself. For instance, dendrite formation & growth on the Zn electrode is a critical issue [20,21] which leads to cell failure from short-circuiting as well as increased parasitic reactions versus the specific surface area of the electrode [22]. This problem is more serious in higher energy density zinc batteries because of higher area of anode – electrolyte interface and higher quantities of Zn in the anode.

Dendrite formation on zinc is driven by differences in overpotential along the surface. Locations with screw dislocations lead to raised edges on the surface of the zinc electrode, and these sites exhibit a higher overpotential compared to the surrounding areas on the electrode [23,24]. There is a higher access to 3D diffusion of ions from the electrolyte on these raised sites resulting in increased rate of reduction than recessed areas on the electrode. Generally, several different approaches have been explored in literature to combat dendritic failure in Zn cells. Firstly, additives can be added into the electrolyte to affect zinc electrodeposition. These additives include surfactants (SDS and Triton-X) [25], polymers [26-28], organic acids such as citric, benzoic and tartaric acids [29-31] and metal ions such as Bi^{3+} and Pb^{2+} [32,33].

They either have affinity for the ions in solution or to the electrode, and they act by hindering the formation of large electrodeposits. Secondly, additives may be added directly to the zinc electrode. Organic binders such as PTFE [34] and PVDF [35] have been shown to reduce the production of dendritic sites, and metal oxides affect the distribution of current density on the electrode surface and can optimize the deposition of zinc [36]. Lastly, the physical structure of the zinc electrode itself can be tailored to minimize dendrite formation. For example, the in-situ growth of a hyper-dendritic zinc foam was shown to form a dense secondary zinc dendrite with particle sizes less than 100 nm [37]. Due to the uniform growth across all the small dendrite structures, there was no runaway growth of large dendrites.

We propose a new gel electrolyte which consists of an aqueous electrolyte containing 2M ZnSO₄ and 1M Li₂SO₄, a fumed silica gelling agent, and short-chain poly(ethyleneglycol) with MW of 300 g·mol⁻¹ (PEG300) as the non-thixotropic gelling agent, for secondary Zn/LiMn₂O₄ batteries. We aim to use a combined approach of controlling the diffusion of Zn²⁺ ions in solution as well as guided deposition by using polymers to restrict reduction and deposition of ions in non-ideal sites. Using a thixotropic silica gelling agent is beneficial to the battery and significantly aids in mitigating dendrite formation [38]. Herein, we show that PEG300 is an effective additive, and can further improve corrosion (54% lesser corrosion current density), dendrite suppression (30% lesser chronoamperometric current density), reliability, and long-term cycling performance (35.78 mAhg⁻¹ higher specific discharge capacity after 300 cycles) over the 5wt.%FS electrolyte.

2. Experimental

2.1. Preparation of batteries

Electrode preparation has already been described in literature [39]. The reference liquid aqueous electrolyte was prepared from $\text{Li}_2\text{SO}_4 \cdot \text{H}_2\text{O}$ (Sigma Aldrich, 98%), $\text{ZnSO}_4 \cdot 7\text{H}_2\text{O}$ (Sigma Aldrich, 98%) and deionized water to obtain a solution containing 1M Li_2SO_4 and 2M ZnSO_4 , pH was adjusted to 4.00 ± 0.05 . The gelled electrolytes are prepared by adding respective quantities of Fumed Silica (7 nm, Sigma Aldrich) and PEG300 (Sigma Aldrich) into the reference electrolyte.

2.2. Electrochemical characterization

The chronoamperometry three-electrode cell consists of *ca.* 2.5 cm^2 of polished zinc (Rotometals) (WE), nickel foam (CE), and SCE (RE). An overpotential of -120 mV vs. Zn^{2+}/Zn was applied for 1 hour using a multi-channel potentiostat (VMP3, Biologic).

For corrosion measurements, a polished Zn strip with area of *ca.* 5 cm^2 (WE), Pt (CE), and SCE (RE) were used. A linear polarization (LP) sweep was applied from -0.020 V to +0.020 V versus the EVT at $0.01 \text{ mV} \cdot \text{s}^{-1}$ using a multi-channel potentiostat (VMP3, Biologic).

The cycling test was implemented on Swagelok-type cells and a bespoke large (7 mA·hour) cell. Each cell contained a $\text{LiMn}_2\text{O}_4/\text{KS-6}/\text{PVdF}$ (86:7:7 wt.%) composite

cathode and a polished zinc metal anode, and an Absorbed Glass Mat (AGM) separator. LiMn_2O_4 , KS-6, and PVdF (HSV 900) are provided by MTI, Imerys Graphite & Carbon, and Kynar[®] (Alchemia), respectively. The areal loading of the active cathode material was $4\text{-}6\text{ mg}\cdot\text{cm}^{-2}$. The electrolytes were injected (by syringe) onto the separator (*ca.* 0.4 g). Battery testing was conducted on a multi-channel battery tester (BTS-5V10mA, Neware). The cells were cycled between 1.4 and 2.1 V at 1 C (1 C is defined as $115\text{ mA}\cdot\text{h}\cdot\text{g}^{-1}$), at $\sim 25\text{ }^\circ\text{C}$.

3. Results and Discussion

Chronoamperometry (CA) was used to physically quantify the rate of zinc growth on a target electrode. This rate is related to the responded CA current density because each Zn^{2+} from the electrolyte will accept 2 electrons to be converted to neutral Zn and deposit on the surface of the working electrode. Under the same overpotential, the absolute value of CA current density and the time duration required for equilibrium are related to the characteristics of the deposit, which can be measured *ex-situ* by microscopy and crystallography. The chronoamperograms of Zn electrodes from the different electrolytes are shown in Figure 1 (a). In the reference electrolyte, the absolute value of current density rapidly increases over time. This trend signifies an increase in surface area as the test proceeds – this is only possible if the aspect ratio of surface features increases. In the 5wt.%FS electrolyte, the absolute current density shows a sharp decrease in value after approximately 150 s such that the final absolute current density is significantly lower ($-6.35\text{ mA}\cdot\text{cm}^{-2}$ vs. $-20.39\text{ mA}\cdot\text{cm}^{-2}$) than the reference electrolyte. This shrinkage points to decreasing aspect ratio of surface

features which will lead to much flatter surface morphology [40]. Introduction of PEG300 to the gel electrolyte significantly inhibits nucleation, 2D and 3D diffusion processes compared to reference electrolyte. This indicates that PEG polymers affect the reduction and diffusion mechanisms of Zn ions, and a decrease in the respective currents may result in highly uniform morphology of the electrode [26]. The concentration of the PEG additive exhibits positive effect on dendrite inhibition: increasing from 1wt.% to 2wt.% shows a slight decrease in the absolute current density ($-5.10 \text{ mA}\cdot\text{cm}^{-2}$ vs. $-4.47 \text{ mA}\cdot\text{cm}^{-2}$).

SEM images of the Zn WE after testing with reference, 5wt.%FS, 4wt.%FS-1wt.%PEG300, and 3wt.%FS-2wt.%PEG300 electrolytes are presented in Figure 2. The reference aqueous electrolyte sample exhibits uncontrolled dendritic growth with large and jagged boulder-type dendrites observable on the surface. In contrast, in the 5wt.%FS gel electrolyte, the surface features are much flatter and more aggregated. The edges of the surface features are also smoother. This observation confirms the chronoamperometry result of the 5%FS gel exhibiting much lower 3D diffusion current after 1 hour. Fumed silica therefore prevents high aspect ratio dendrites from forming [40]. While this is highly desired, the corrosion rate of Zn in this electrolyte is increased compared to the reference electrolyte [41].

In the 4wt.%FS-1wt.%PEG300 and 3wt.%FS-2wt.%PEG300 electrolytes, deposits have a flake-type morphology instead of boulder-type observed without PEG. These features are also much smaller ($< 1 \mu\text{m}$) than those observed without PEG ($> 10 \mu\text{m}$). Increasing the concentration of PEG300 in the gel decreases the size

of the dendrite flakes. This size difference explains the decrease in absolute current density between the 4wt.%FS-1wt.%PEG300 and 3wt.%FS-2wt.%PEG300 electrolytes.

Tafel extrapolation was applied to linear polarization of zinc to obtain the corrosion potentials and current densities in different electrolytes (Figure 1 (b), table 1). It is immediately evident that the corrosion on the Zn electrode is much higher in 5wt.%FS gel electrolyte than in the reference aqueous system (0.0073 V and 2.571 $\mu\text{A}\cdot\text{cm}^{-2}$ lower potential and higher current density, respectively). The increased corrosion current signifies a higher rate of reaction which is harmful to the electrode in the long-term. The 4wt.%FS-1wt.%PEG300 and 3wt.%FS-2wt.%PEG300 electrolytes exhibit both lower corrosion current densities as well as higher (more positive) equilibrium potentials. The corrosion current density decreases significantly, from $5.980\pm 0.714 \mu\text{A}\cdot\text{cm}^{-2}$ to $4.952\pm 0.515 \mu\text{A}\cdot\text{cm}^{-2}$, when increasing the PEG300 content from 1wt.% to 2wt.%, respectively, in the electrolyte. This result proves PEG300 is a substantial corrosion inhibitor and can be used in lieu of other toxic additives such as Pb^{2+} [42].

Hydrogen gas evolution – the counter process of corrosion – is significantly reduced in the PEG-FS gel electrolytes [43]. Decreased hydrogen gas production has two effects: firstly, it improves the safety of the battery since there will be much less internal pressure buildup, and secondly, more H^+ ions are retained in the gel hence preserving the pH of the electrolyte. Overall, these advantages improve the lifetime and reliability of aqueous batteries.

Figure 1 (c) presents the results of the cyclability test following a CC-CV protocol (0.1 C current cut-off). After 300 cycles, the gelled batteries exhibit 10-12% higher capacity retention than the reference batteries. The best performing system, 4wt.%FS-1wt.%PEG300, was then selected for extended testing in the bespoke large battery. In this test, as shown in Figure 1 (d), the reference electrolyte achieves an initial capacity of $114.00 \pm 4.26 \text{ mAh.g}^{-1}$ while the 4wt.%FS-1wt.%PEG300 battery is able to reach up to $141.00 \pm 1.29 \text{ mAh.g}^{-1}$ at the initial cycle. After 1000 cycles, the reference battery shows 15% of capacity retention, 39% less than the gelled system.

Additionally, the rapid decline in discharge capacity of the reference large battery after approximately 730 cycles, together with the highly fluctuating coulombic efficiency, shows the failure of the system from dendrite formation. The trend of increasing difference in capacity retention between the aqueous and gel electrolytes during cycling shows the impact of PEG300 on lifespan and reliability of batteries.

Voltage profiles at 1st, 500th, and 1000th cycles of both reference and gelled batteries are plotted in Figure 1 (e) and (f), respectively. They share the same shape, which is characteristic of LiMn_2O_4 , with two plateaus corresponding to a two-step Li^+ intercalation process [44–46]. The gelled battery offers higher coulombic efficiency at first cycle, and exhibits higher discharge capacity over the entire cycling test. The 4wt.%FS-1wt.%PEG300 electrolyte only loses 10% discharge capacity between 500 and 1000 cycles, while the reference electrolyte experiences a 58% capacity decline in the same period. This result reinforces the benefit of PEG300 in extending cycling lifespan.

Figure 3 (a and b) show low magnification SEM micrographs of the large battery anodes post-cycling, for the first time. While the anode from the 4wt.%FS-1wt.%PEG300 system has reasonable dendrite growth on the surface, large holes were observed in some sections of the anode from the reference system. This is correlated to the increased corrosion in the reference system which leads to the rapid degradation of the Zn anode during operation. Figure 3 (c and d) show higher magnification SEM micrographs of the cycled anodes. Both anodes show typical layered zinc deposits signifying net growth of the anode over time. However, the anode from the reference battery exhibits much larger features (8-10 μm) while those from the PEG-FS gel anode are much smaller (2-3 μm). This gives physical evidence to aforementioned observation of battery failure from dendrite formation. Lastly, Figure 3 (e and f) show the cathode surface post-cycling. No major differences in the morphology of the two cathodes were observed leading us to conclude that the interactions of the PEG gel electrolyte are solely with the zinc anode.

4. Conclusions

A new thixotropic gel electrolyte containing fumed silica and PEG300 as the corrosion inhibitor, dendrite suppressor, and gelling agent is successfully prepared. Chronoamperometry and *ex-situ* scanning electron microscopy studies confirm that this electrolyte protects the Zn electrode from excessive dendritic Zn deposits. The addition of PEG300 to the gelled battery increases reliability, exhibiting 27-40% lower corrosion current density on the Zn anode. In comparison to the reference battery, the gelled battery exhibits significantly higher cycling performance after 300

cycles at 1 C rate (12% higher capacity retention) and 39% higher capacity retention after 1000 cycles in the large battery. This shows great prospect for scale-up of this battery for use in large energy storage systems.

Acknowledgments

This research was financially supported by Positec Canada Ltd, Mitacs (IT06145).

Declaration

The authors declare no competing interests.

References

- [1] L. Gaiser, K.E. Heusler, Die kinetik der zinkelektrode in zinkperchloratlösungen, *Electrochim. Acta.* 15 (1970) 161. doi:10.1016/0013-4686(70)90016-2.
- [2] F. Wang, O. Borodin, T. Gao, X. Fan, W. Sun, F. Han, A. Faraone, J.A. Dura, K. Xu, C. Wang, Highly reversible zinc metal anode for aqueous batteries, *Nat. Mater.* 17 (2018) 543–549. doi:10.1038/s41563-018-0063-z.
- [3] M.M. Gross, A. Manthiram, Rechargeable Zinc-Aqueous Polysulfide Battery with a Mediator-Ion Solid Electrolyte, *ACS Appl. Mater. Interfaces.* 10 (2018) 10612–10617. doi:10.1021/acsami.8b00981.
- [4] J.H. Park, N.M. Schneider, D.A. Steingart, H. Deligianni, S. Kodambaka, F.M. Ross, Control of Growth Front Evolution by Bi Additives during ZnAu Electrodeposition, *Nano Lett.* 18 (2018) 1093–1098.

- doi:10.1021/acs.nanolett.7b04640.
- [5] S. Clark, A. Latz, B. Horstmann, A Review of Model-Based Design Tools for Metal-Air Batteries, *Batteries*. 4 (2018) 5. doi:10.3390/batteries4010005.
- [6] J. Zhang, J. Zhao, H. Du, Z. Zhang, S. Wang, G. Cui, Amide-based molten electrolyte with hybrid active ions for rechargeable Zn batteries, *Electrochim. Acta*. 280 (2018) 108–113. doi:10.1016/j.electacta.2018.05.107.
- [7] W. Dong, J.-L. Shi, T.-S. Wang, Y.-X. Yin, C.-R. Wang, Y.-G. Guo, 3D zinc@carbon fiber composite framework anode for aqueous Zn–MnO₂ batteries, *RSC Adv.* 8 (2018) 19157–19163. doi:10.1039/C8RA03226B.
- [8] F. El-Taib Heikal, W.R. Abd-Ellatif, N.S. Tantawy, A.A. Taha, Impact of pH and temperature on the electrochemical and semiconducting properties of zinc in alkaline buffer media, *RSC Adv.* 8 (2018) 3816–3827. doi:10.1039/C7RA12723E.
- [9] J. Duan, W. Xie, P. Yang, J. Li, G. Xue, Q. Chen, B. Yu, R. Liu, J. Zhou, Tough hydrogel diodes with tunable interfacial adhesion for safe and durable wearable batteries, *Nano Energy*. 48 (2018) 569–574. doi:10.1016/j.nanoen.2018.04.014.
- [10] J. Li, M.K. Aslam, C. Chen, One-Pot Hydrothermal Synthesis of Porous α -Ni(OH)₂/C Composites and Its Application in Ni/Zn Alkaline Rechargeable Battery, *J. Electrochem. Soc.* 165 (2018) A910–A917. doi:10.1149/2.0721805jes.

- [11] A. Khor, P. Leung, M.R. Mohamed, C. Flox, Q. Xu, L. An, R.G.A. Wills, J.R. Morante, A.A. Shah, Review of zinc-based hybrid flow batteries: From fundamentals to applications, *Mater. Today Energy*. 8 (2018) 80–108. doi:10.1016/J.MTENER.2017.12.012.
- [12] S. Maazi, A.H. Navarchian, M. Khosravi, P. Chen, Effect of poly(vinylidene fluoride)/poly(vinyl acetate) blend composition as cathode binder on electrochemical performances of aqueous Li-ion battery, *Solid State Ionics*. 320 (2018) 84–91. doi:10.1016/J.SSI.2018.02.033.
- [13] J. Zhi, K. Bertens, A.Z. Yazdi, P. Chen, Acrylonitrile copolymer/graphene skinned cathode for long cycle life rechargeable hybrid aqueous batteries at high-temperature, *Electrochim. Acta*. 268 (2018) 248–255. doi:10.1016/J.ELECTACTA.2018.02.098.
- [14] X. Liu, M. Park, M.G. Kim, S. Gupta, X. Wang, G. Wu, J. Cho, High-performance non-spinel cobalt-manganese mixed oxide-based bifunctional electrocatalysts for rechargeable zinc-air batteries, *Nano Energy*. (2015). doi:10.1016/j.nanoen.2015.11.030.
- [15] J. Zhou, L. Shan, Z. Wu, X. Guo, G. Fang, S. Liang, Investigation of V_2O_5 as a low-cost rechargeable aqueous zinc ion battery cathode, *Chem. Commun*. 54 (2018) 4457–4460. doi:10.1039/C8CC02250J.
- [16] S. Yang, M. Zhang, X. Wu, X. Wu, F. Zeng, Y. Li, S. Duan, D. Fan, Y. Yang, X. Wu, The excellent electrochemical performances of $ZnMn_2O_4/Mn_2O_3$: The

- composite cathode material for potential aqueous zinc ion batteries, J. Electroanal. Chem. 832 (2019) 69–74. doi:10.1016/j.jelechem.2018.10.051.
- [17] J. Cui, X. Wu, S. Yang, C. Li, F. Tang, J. Chen, Y. Chen, Y. Xiang, X. Wu, Z. He, Cryptomelane-Type $\text{KMn}_8\text{O}_{16}$ as Potential Cathode Material — for Aqueous Zinc Ion Battery, *Front. Chem.* 6 (2018) 352. doi:10.3389/fchem.2018.00352.
- [18] C. Zhu, G. Fang, J. Zhou, J. Guo, Z. Wang, C. Wang, J. Li, Y. Tang, S. Liang, Binder-free stainless steel@ Mn_3O_4 nanoflower composite: a high-activity aqueous zinc-ion battery cathode with high-capacity and long-cycle-life, J. Mater. Chem. A. 6 (2018) 9677–9683. doi:10.1039/C8TA01198B.
- [19] X. Wu, Y. Xiang, Q. Peng, X. Wu, Y. Li, F. Tang, R. Song, Z. Liu, Z. He, X. Wu, Green-low-cost rechargeable aqueous zinc-ion batteries using hollow porous spinel ZnMn_2O_4 as the cathode material, J. Mater. Chem. A. 5 (2017) 17990–17997. doi:10.1039/C7TA00100B.
- [20] K. Wang, P. Pei, Y. Wang, C. Liao, W. Wang, S. Huang, Advanced rechargeable zinc-air battery with parameter optimization, *Appl. Energy.* 225 (2018) 848–856. doi:10.1016/j.apenergy.2018.05.071.
- [21] F. Liu, H.-J. Chung, J.A.W. Elliott, Freezing of Aqueous Electrolytes in Zinc–Air Batteries: Effect of Composition and Nanoscale Confinement, *ACS Appl. Energy Mater.* 1 (2018) 1489–1495. doi:10.1021/acsaem.7b00307.

- [22] K.E.K. Sun, T.K.A. Hoang, T.N.L. Doan, Y. Yu, X. Zhu, Y. Tian, P. Chen, Suppression of Dendrite Formation and Corrosion on Zinc Anode of Secondary Aqueous Batteries, *ACS Appl. Mater. Interfaces*. 9 (2017) 9681–9687.
doi:10.1021/acsami.6b16560.
- [23] J.W. Diggle, A.R. Despic, J.O. Bockris, The Mechanism of the Dendritic Electrocrystallization of Zinc, *J. Electrochem. Soc.* 116 (1969) 1503.
doi:10.1149/1.2411588.
- [24] K.I. Popov, P.M. Živković, N.D. Nikolić, Electrochemical aspects of formation of dendrites, *Zast. Mater.* 57 (2016) 55–62. doi:10.5937/ZasMat1601055P.
- [25] J. Kan, H. Xue, S. Mu, Effect of inhibitors on Zn-dendrite formation for zinc-polyaniline secondary battery, *J. Power Sources*. 74 (1998) 113.
doi:10.1016/S0378-7753(98)00040-8.
- [26] A. Mitha, A.Z. Yazdi, M. Ahmed, P. Chen, Surface Adsorption of Polyethylene Glycol to Suppress Dendrite Formation on Zinc Anodes in Rechargeable Aqueous Batteries, *ChemElectroChem*. (2018). doi:10.1002/celec.201800572.
- [27] S.J. Banik, SUPPRESSING DENDRITIC GROWTH DURING ZINC ELECTRODEPOSITION USING POLYETHYLENIMINE AS AN ELECTROLYTE ADDITIVE FOR RECHARGEABLE ZINC BATTERIES, Doctoral Thesis, Case Western University, 2016.

- [28] T. Akiyama, S. Kobayashi, J. Ki, T. Ohgai, H. Fukushima, Role of polyethylene glycol in electrodeposition of zinc–chromium alloys, *J. Appl. Electrochem.* 30 (2000) 817–822. doi:10.1023/A:1004093531922.
- [29] O. Aaboubi, J. Douglade, X. Abenaqui, R. Boumedmed, J. VonHoff, Influence of tartaric acid on zinc electrodeposition from sulphate bath, *Electrochim. Acta.* 56 (2011) 7885–7889. doi:10.1016/J.ELECTACTA.2011.05.121.
- [30] H. Natter, R. Hempelmann, Nanocrystalline Copper by Pulsed Electrodeposition: The Effects of Organic Additives, Bath Temperature, and pH, *J. Phys. Chem.* 100 (1996) 19525–19532. doi:10.1021/JP9617837.
- [31] J.-Y. Lee, J.-W. Kim, M.-K. Lee, H.-J. Shin, H.-T. Kim, S.-M. Park, Effects of Organic Additives on Initial Stages of Zinc Electroplating on Iron, *J. Electrochem. Soc.* 151 (2004) C25. doi:10.1149/1.1627344.
- [32] J.M. Wang, L. Zhang, C. Zhang, J.Q. Zhang, Effects of bismuth ion and tetrabutylammonium bromide on the dendritic growth of zinc in alkaline zincate solutions, *J. Power Sources.* 102 (2001) 139–143. doi:10.1016/S0378-7753(01)00789-3.
- [33] F. Mansfeld, S. Gilman, The Effect of Lead Ions on the Dissolution and Deposition Characteristics of a Zinc Single Crystal in 6N KOH, *J. Electrochem. Soc.* 117 (1970) 588. doi:10.1149/1.2407584.

- [34] K. Bass, P.J. Mitchell, G.D. Wilcox, J. Smith, The electrodeposition of zinc onto graphitic carbon substrates from alkaline electrolytes, *J. Power Sources*. 24 (1988) 21–29. doi:10.1016/0378-7753(88)80086-7.
- [35] H. Li, C. Xu, C. Han, Y. Chen, C. Wei, B. Li, F. Kang, Enhancement on Cycle Performance of Zn Anodes by Activated Carbon Modification for Neutral Rechargeable Zinc Ion Batteries, *J. Electrochem. Soc.* 162 (2015) A1439–A1444. doi:10.1149/2.0141508jes.
- [36] B.-S. Lee, S. Cui, X. Xing, H. Liu, X. Yue, V. Petrova, H.-D. Lim, R. Chen, P. Liu, Dendrite Suppression Membranes for Rechargeable Zinc Batteries, *ACS Appl. Mater. Interfaces*. 10 (2018) 38928–38935. doi:10.1021/acsami.8b14022.
- [37] M. Chamoun, B.J. Hertzberg, T. Gupta, D. Davies, S. Bhadra, B. Van Tassell, C. Erdonmez, D.A. Steingart, Hyper-dendritic nanoporous zinc foam anodes, *NPG Asia Mater.* 7 (2015) e178–e178. doi:10.1038/am.2015.32.
- [38] T.K.A. Hoang, T.N.L. Doan, J.H. Cho, J.Y.J. Su, C. Lee, C. Lu, P. Chen, Sustainable Gel Electrolyte Containing Pyrazole as Corrosion Inhibitor and Dendrite Suppressor for Aqueous Zn/LiMn₂O₄ Battery, *ChemSusChem*. 10 (2017) 2816–2822. doi:10.1002/cssc.201700441.
- [39] T.K.A. Hoang, T.N.L. Doan, C. Lu, M. Ghaznavi, H. Zhao, P. Chen, Performance of thixotropic gel electrolytes in the rechargeable aqueous Zn/LiMn₂O₄ battery, *ACS Sustain. Chem. Eng.* 2018 (2017) 1804.

- doi:10.1021/acssuschemeng.6b02553.
- [40] H. Inoue, M. Kurosaki, S. Nohara, Deposition of Zinc in Polymer Hydrogel Electrolyte, in: 214th ECS Meet., The Electrochemical Society. (2008).
- [41] T.K.A. Hoang, M. Acton, H.T.H. Chen, Y. Huang, T.N.L. Doan, P. Chen, Sustainable gel electrolyte containing Pb^{2+} as corrosion inhibitor and dendrite suppressor for the zinc anode in the rechargeable hybrid aqueous battery, *Mater. Today Energy*. 4 (2017) 34–40. doi:10.1016/J.MTENER.2017.03.003.
- [42] A. Zgoła-Grzeškowiak, T. Grzeškowiak, J. Zembrzuska, Z. Łukaszewski, Comparison of biodegradation of poly(ethylene glycol)s and poly(propylene glycol)s, *Chemosphere*. 64 (2006) 803–809.
doi:10.1016/j.chemosphere.2005.10.056.
- [43] J.-S. Lee, S. Tai Kim, R. Cao, N.-S. Choi, M. Liu, K.T. Lee, J. Cho, Metal-Air Batteries with High Energy Density: Li-Air versus Zn-Air, *Adv. Energy Mater.* 1 (2011) 34–50. doi:10.1002/aenm.201000010.
- [44] Z. Bakenov, I. Taniguchi, Electrochemical performance of nanostructured $LiM_xMn^{2-x}O_4$ ($M = Co$ and Al) powders at high charge–discharge operations, *Solid State Ionics*. 176 (2005) 1027–1034. doi:10.1016/J.SSI.2005.02.004.
- [45] M.M. Thackeray, P.J. Johnson, L.A. de Picciotto, P.G. Bruce, J.B. Goodenough, Electrochemical extraction of lithium from $LiMn_2O_4$, *Mater. Res. Bull.* 19 (1984) 179–187. doi:10.1016/0025-5408(84)90088-6.

[46] R. Benedek, M.M. Thackeray, Reaction Energy for LiMn_2O_4 Spinel

Dissolution in Acid, *Electrochem. Solid-State Lett.* 9 (2006) A265.

doi:10.1149/1.2188071.

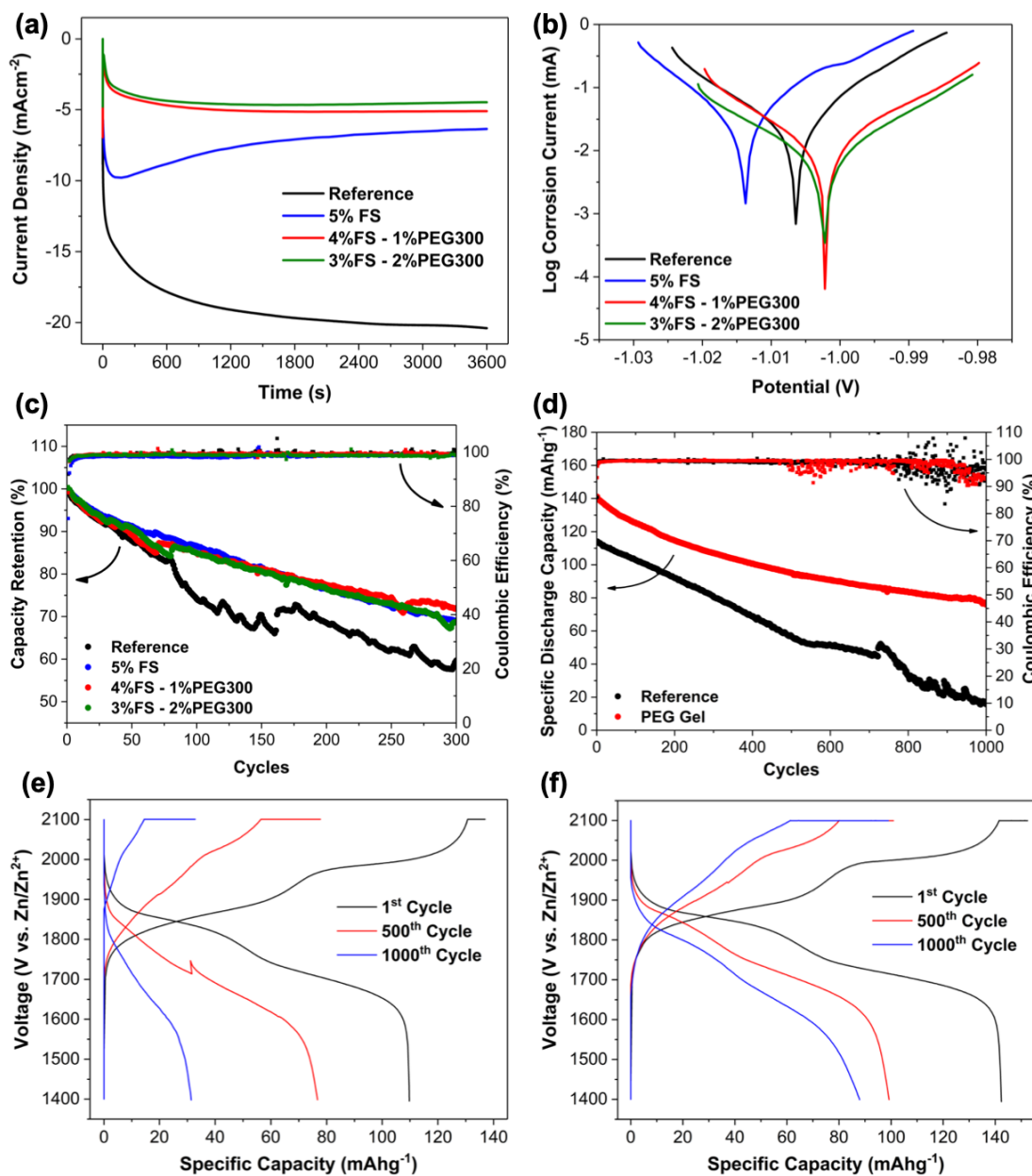


Figure 1: (a) Chronoamperometry and (b) Linear polarization curves of zinc electrodes in different electrolytes. Cycling performance of (c) Swagelok and (d) Large batteries. Large battery voltage profiles of e) Reference, and f) 4%FS-1%PEG300 electrolytes.

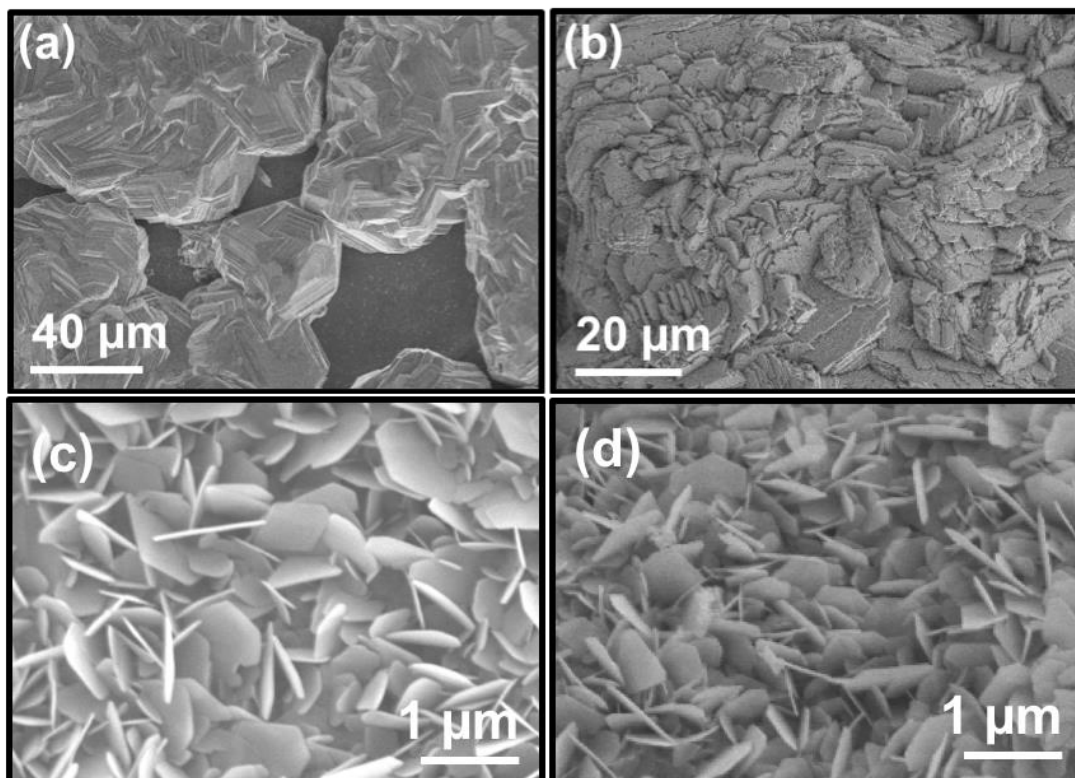


Figure 2: SEM images of post-chronoamperometry zinc electrodes from: (a) reference 1M Li_2SO_4 -2M ZnSO_4 , (b) 5% FS, (c) 4% FS-1% PEG300, (d) 3% FS-2% PEG300 electrolytes

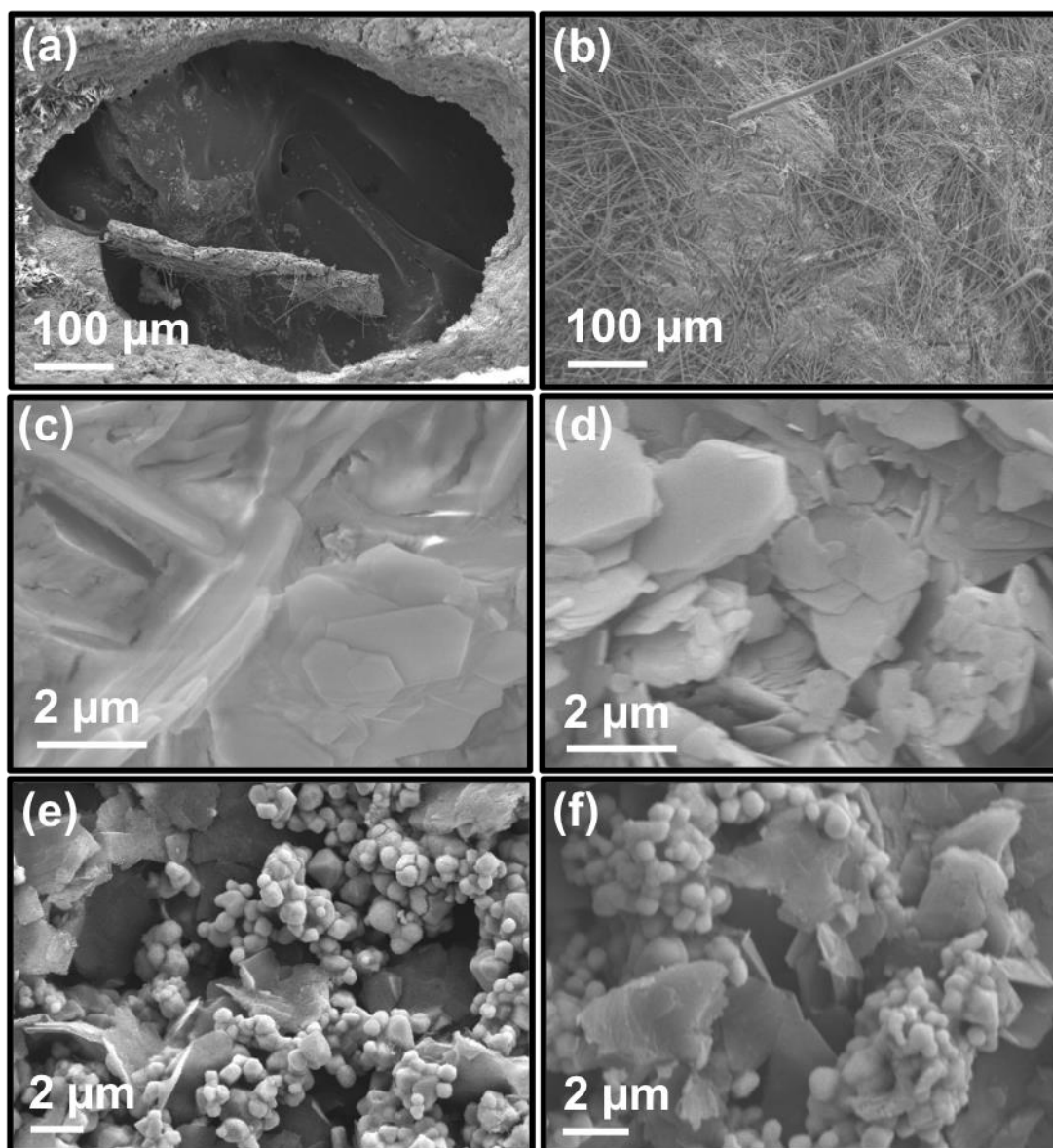
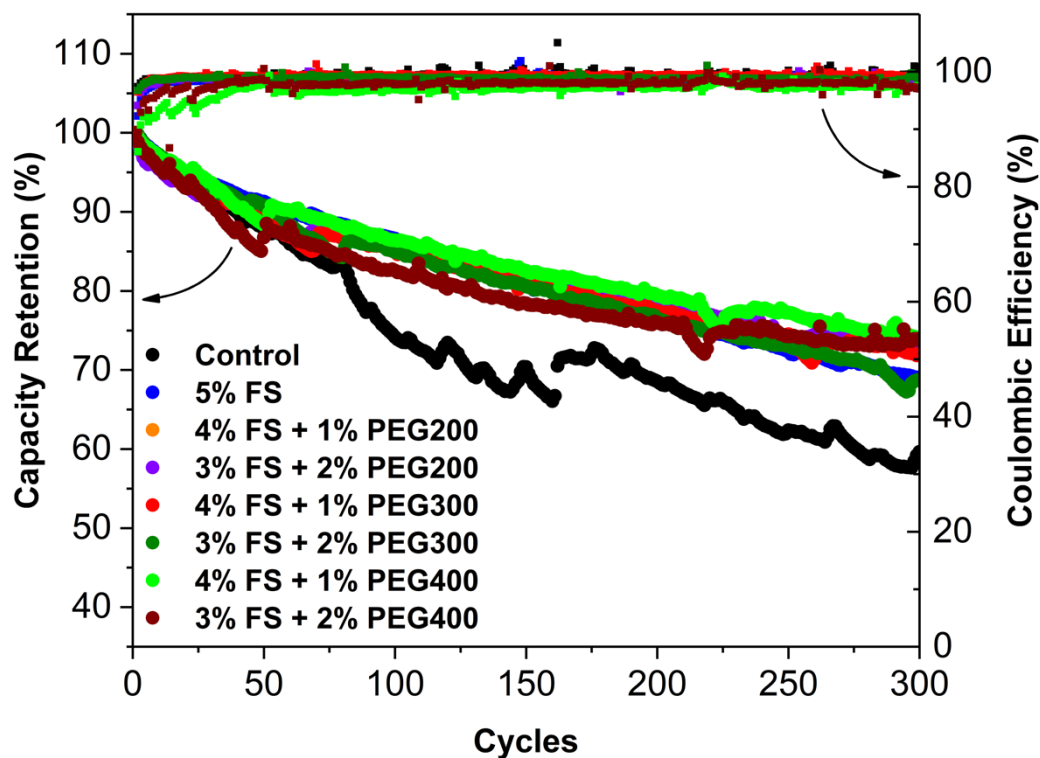


Figure 3: SEM images of large battery anodes after 1000 cycles from (a and c) Reference and (b and d) 4%FS-1%PEG300 electrolytes. SEM images of large battery cathodes after 1000 cycles from (e) Reference and (f) 4%FS-1%PEG300 electrolytes

Table 1: Corrosion performance of zinc in different electrolytes.

Electrolyte	Corrosion Potential (mV)	Corrosion Current ($\mu\text{A}\cdot\text{cm}^{-2}$)
Ref	-1006.6 \pm 0.1	8.237 \pm 0.057
5wt.%FS	-1013.9 \pm 0.7	10.808 \pm 0.692
4wt.%FS-1wt.%PEG	-1001.95 \pm 0.35	5.980 \pm 0.714
3wt.%FS-2wt.%PEG	-1002.05 \pm 0.42	4.952 \pm 0.515

Supplementary Figures**Figure S1:** Cycling performance of ReHAB Swagelok cells containing different gel electrolytes

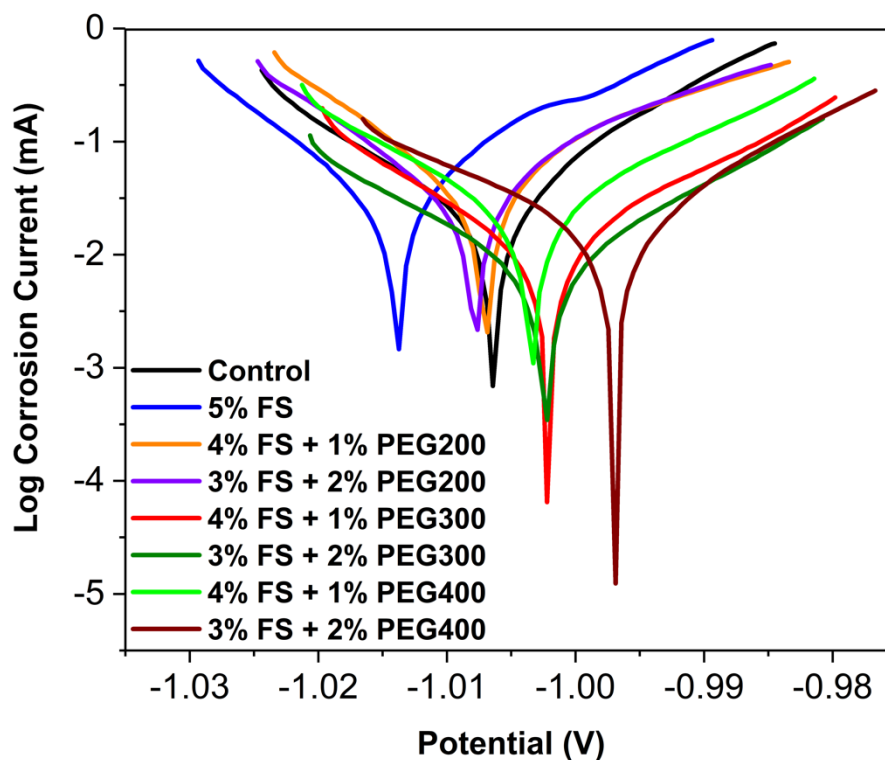


Figure S2: Linear polarization of zinc electrodes in different gel electrolytes

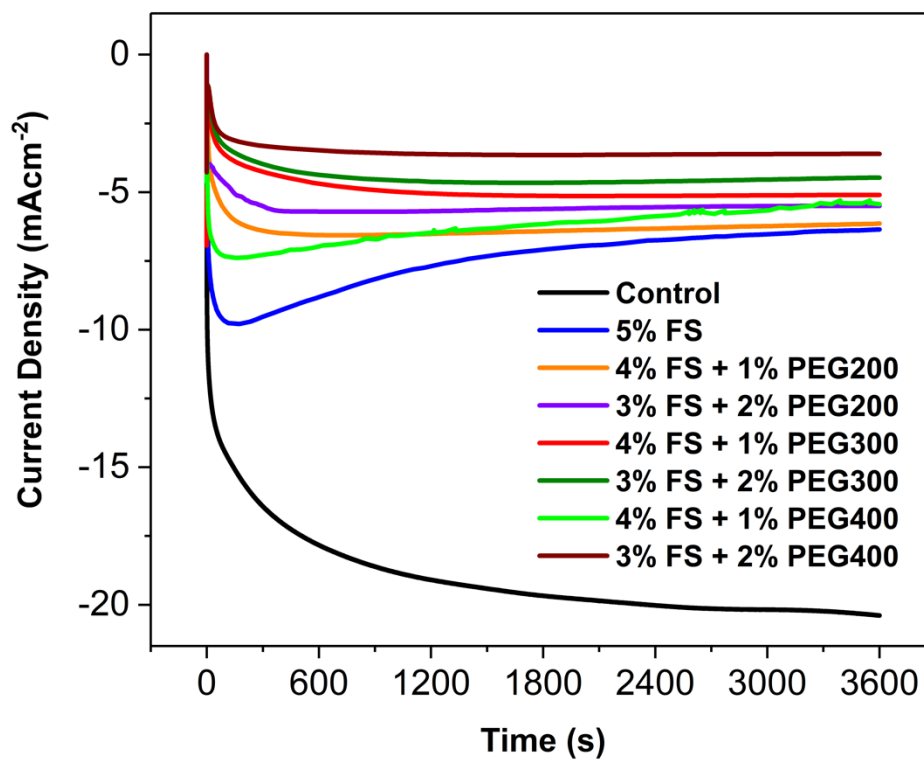
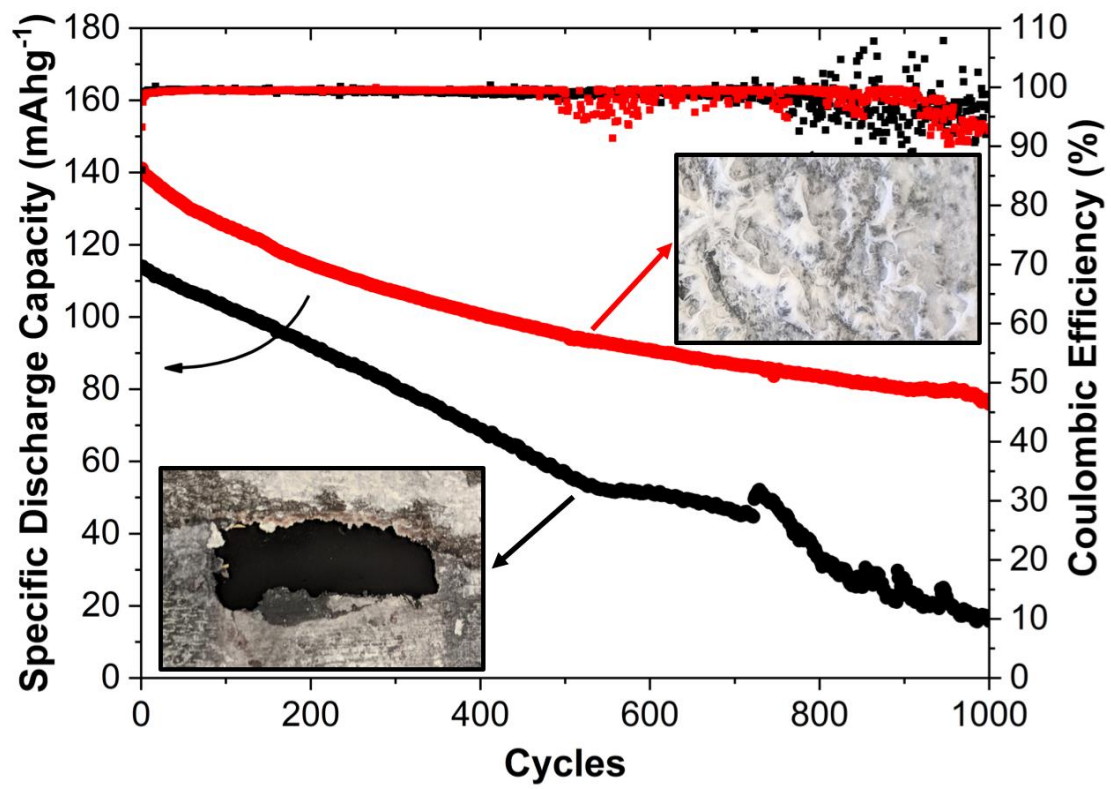


Figure S3: Chronoamperometry of zinc electrodes in different gel electrolytes



Graphical abstract

Highlights

We report the following improvements through the use of the novel gelled electrolyte:

1. 27% decrease in the corrosion current density of the zinc electrode.
2. 75% reduction in the chronoamperometric current density of the zinc electrode compared to the reference, indicating a vast improvement in dendrite inhibition.
3. 39% improvement in the capacity retention after 1000 cycles compared to the control when measuring cycling performance in our bespoke large battery system.